Iridium–Imine and –Amine Complexes Relevant to the (*S*)-Metolachlor Process: Structures, Exchange Kinetics, and C–H Activation by Ir^I Causing Racemization**

Romano Dorta,*[a] Diego Broggini,[b] Reinhard Kissner,[c] and Antonio Togni[c]

Abstract: Iridium complexes of DMA-imine [2,6-dimethylphenyl-1′-methyl-2′-methoxyethylimine, **1a**) and (*R*)-DMA-amine [(1′*R*)-2,6-dimethylphenyl-1′-methyl-2′-methoxyethylamine, **2a**] that are relevant to the catalytic imine hydrogenation step of the Syngenta (*S*)-Metolachlor process were synthesized: metathetical exchange of $[Ir_2Cl_2(cod)_2]$ (cod = 1,5-cyclooctadiene) with $[Ag(\mathbf{1a})_2]BF_4$ and $[Ag((R)\text{-}\mathbf{2a})_2]BF_4$ afforded $[Ir(cod)(\kappa^{2}\text{-}\mathbf{1a})]BF_4$ (**11**) and $[Ir(cod)(\kappa^{2}\text{-}(R)\text{-}\mathbf{2a})]BF_4$ ((*R*)-**19**)), respectively. These complexes were then used in stopped-flow experiments to study the displacement of amine **2a** from complex **19** by imine **1a** to form the imine complex **11**, thus modeling the product/substrate exchange step in the catalytic cycle. The data suggest a two-step associative mechanism characterized by $k_1 = (2.6 \pm 0.3) \times 10^2\,M^{-1}s^{-1}$ and $k_2 = (4.3 \pm 0.6) \times 10^{-2}\,s^{-1}$ with the respective activation energies $E_{A1} = (7.5 \pm 0.6)\,kJ\,mol^{-1}$ and $E_{A2} = (37 \pm 3)\,kJ\,mol^{-1}$. Furthermore, complex **11** reacted with H_2O to afford the hydrolysis product $[Ir(cod)(\eta^{6}\text{-}2,6\text{-dimethylaniline})]BF_4$ (**12**), and with I_2 to liberate quantitatively the DMA-iminium salt **14**. On the other hand, the chiral amine complex (*R*)-**19** formed the optically inactive η^6-bound compound $[Ir(cod)(\eta^{6}\text{-}rac\text{-}\mathbf{2a})]BF_4$ (*rac*-**18**) upon dissolution in THF at room temperature, presumably via intramolecular C–H activation. This racemization was found to be a two-step event with $k'_1 = 9.0 \times 10^{-4}\,s^{-1}$ and $k_2 = 2.89 \times 10^{-5}\,s^{-1}$, featuring an optically active intermediate prior to sp^3 C–H activation. Compounds **11**, **12**, *rac*-**18**, and (*R*)-**19** were structurally characterized by single-crystal X-ray analyses.

Keywords: C–H activation · exchange kinetics · iridium · metolachlor · N ligands

Introduction

To date, Syngenta AG produces the chiral herbicide (*S*)-Metolachlor [*N*-(1′-methyl-2′-methoxyethyl)-*N*-chloroacetyl-2-ethyl-6-methylaniline, (**3**)][1] in amounts of more than 10000 t per annum in about 80% optical purity.[2–4] The "chiral switch" from the racemate to an enantiomerically enriched form (trademark Dual-Magnum) took place in 1997 after it was found that the two atropisomers (resulting from hindered rotation around the C_{Ar}–N axis) of the (1*S*)-**3** enantiomer are responsible for most of the biological activity.[5] The key step in the Metolachlor synthesis is iridium-catalyzed enantioselective imine hydrogenation[6–8] (Scheme 1). The soluble catalyst system, which we studied in some detail,[9] is a combination of $[Ir_2Cl_2(cod)_2]$ (cod = 1,5-cyclooc-

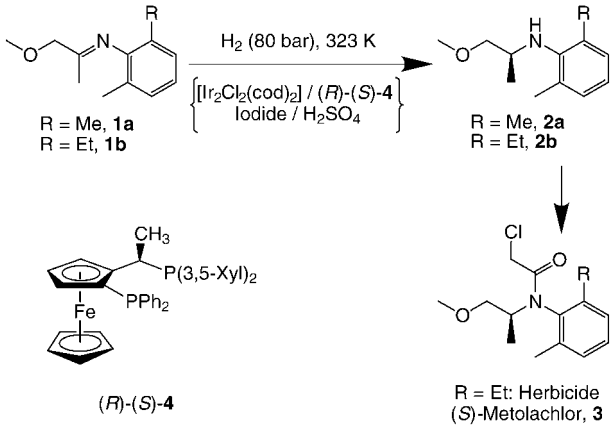

Scheme 1. Industrial synthesis of Metolachlor (Syngenta).

[a] Prof. Dr. R. Dorta
Departamento de Química, Universidad Simón Bolívar
Caracas 1080A (Venezuela)
Fax: (+58) 212-9063961
E-mail: rdorta@usb.ve

[b] Dr. D. Broggini
Department of Chemistry and Biochemistry, University of California
Santa Barbara, CA 93106–9510 (USA)

[c] Dr. R. Kissner, Prof. Dr. A. Togni
Laboratory of Inorganic Chemistry, Swiss Federal Institute of Technology
ETH Hönggerberg, 8093 Zürich (Switzerland)

[**] Part II. Part I: see ref. [9]. The experimental part of this work was carried out at ETH Zürich.

DOI: 10.1002/chem.200306008

tadiene), the chiral ferrocenyldiphosphine Xyliphos (**4**), tetrabutylammonium iodide (TBAI), and sulfuric acid. MEA-imine **1b** is hydrogenated under 80 bar hydrogen pressure at 323 K and at a substrate/catalyst ratio exceeding 10^6 to yield MEA-amine **2b** in 79% *ee* and with an initial turnover frequency that is said to exceed $1.8\times10^6\ h^{-1}$.[3] Currently, this hydrogenation not only represents the largest scale enantioselective catalytic process in use in industry, but it is also one of the fastest homogeneous systems known, second only to certain homogeneous Ziegler–Natta polymerization catalysts[10] and Noyori's ruthenium hydrogenation catalysts.[11] A possible hydrogenation cycle starts with the coordination of imine **1** to an Ir hydride complex to form imine adduct **5** (Scheme 2). Migratory insertion of the

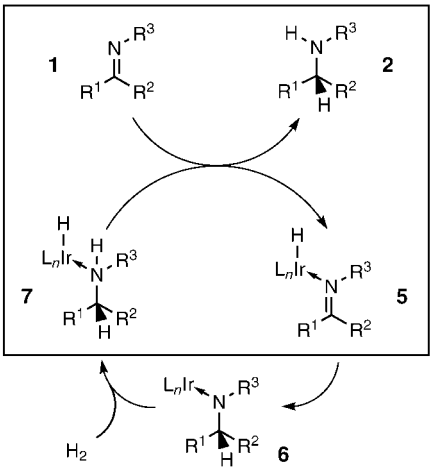

Scheme 2. Proposed cycle of the iridium-catalyzed imine hydrogenation.

C=N bond into the Ir–H bond leads to an iridium–amide function (**6**) which was shown by Fryzuk et al. to add dihydrogen by heterolytic activation.[12] The resulting iridium–hydrido–amino species **7** liberates amine **2** upon coordination of an incoming substrate molecule (**1**). The catalytic cycle is thought to be Ir^{III}-based and Ng Cheong Chan and Osborn originally proposed a dissociative amine/imine exchange sequence.[6]

Iridium xyliphos complexes corresponding to intermediate **5** have recently been isolated and fully characterized, whereas iridium–xyliphos–amido (**6**) and –amino (**7**) complexes have eluded isolation in pure form so far.[9] Therefore, we opted to study simpler, phosphine-free model compounds for intermediates **5** and **7** based on the Ir^{I}(cod) fragment. DMA-imine **1a** and DMA-amine **2a** were used as close model compounds for MEA-imine and MEA-amine (**1b** and **2b**), respectively, to avoid complications caused by atropisomerism of iridium-bound **1b** and **2b** (imine **1a** behaves in much the same way as **1b** under the aforementioned hydrogenation conditions[13]). Herein, we present the synthesis and full characterization of Ir^{I}(cod) DMA-amine and DMA-imine complexes which then allowed us to model the upper part of the cycle depicted in Scheme 2. The analysis of the kinetic data of the amine/imine substitution on the iridium center allowed us to propose an associative mechanism. Furthermore, the three potential metal coordinating modes of imines **1a**,**b** and amines **2a**,**b** (Figure 1) were demonstrated in reactivity studies, and all were assessed by X-ray crystallography. Finally, an unprecedented sp^3 C–H activation by the Ir^{I}(cod) fragment was inferred from the racemization of coordinated optically pure amine **2a**.

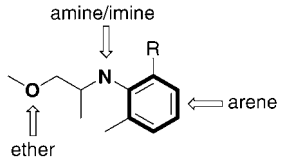

Figure 1. Possible coordinating functions of **1** and **2**. R = Me, Et.

Results and Discussion

Synthesis and reactivity of DMA-imine complexes: Imine **1a** is accessible through the condensation of methoxyacetone and 2,6-dimethylaniline in good yields. Imine **1a** was isolated as a *cis–trans* equilibrium mixture in a 16:84 ratio at room temperature [Eq. (1)]. First attempts to synthesize iridium-imine adducts by reacting $[Ir_2Cl_2(coe)_4]$ (coe = cyclooctene) with a large excess of **1a** in the presence of two equivalents of $AgBF_4$ failed. It showed instead that **1a** cleanly complexed the silver cation leaving the starting $[Ir_2Cl_2(coe)_4]$ unaltered. In a separate synthesis, the silver–imine complex **10** was obtained as a white powder on a gram scale in 90% yield by reacting a toluene solution of $AgBF_4$ with two equivalents of imine **1a** according to Equation (2).[9] Complex **10** showed good solubility in CH_2Cl_2 and, to a lesser extent, in toluene and benzene. CH_2Cl_2 solutions decomposed within a day to form AgCl. The ^{1}H NMR spectrum of **10** indicated that only one of the *cis–trans* isomers of **1a** coordinated to the silver cation and that the coordination of **1a** did not significantly change its chemical shifts. This silver–imine complex transmetalated quantitatively with $[Ir_2Cl_2(cod)_2]$ to yield the cationic iridium-imine adduct **11** [Eq. (3)]. The ^{1}H NMR spectrum of **11** supported a bidentate coordination mode of **1a**, and again only one isomer was observed. The resonance of the methoxy protons of coordinated **1a** was shifted downfield by about 0.5 ppm to $\delta = 3.95$ ppm. The imine-methyl protons resonated at $\delta = 1.89$ ppm and the methylene protons at $\delta = 5.40$ ppm as compared to $\delta = 1.66$ and 4.20 ppm, respectively, in free **1a**.

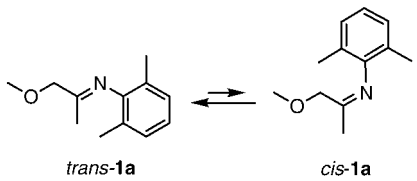

(1)

$$AgBF_4 + 2\,\mathbf{1a} \xrightarrow{\text{toluene}} [Ag(\mathbf{1a})_2]BF_4\ (\mathbf{10}) \qquad (2)$$

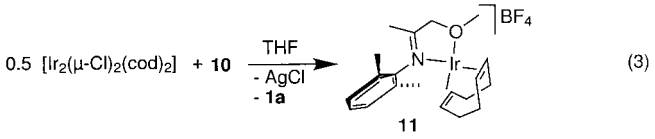

Crystals suitable for X-ray crystallography were grown by slowly cooling a saturated THF solution of **11** from 333 K to room temperature. We noticed a reproducible tendency of **11** to form hexagonal tubuli with diameters ranging from 1 to 2 mm. Noteworthy are the rare trigonal space group and the large, "pizza box"-shaped unit cell ($a=31.040(12)$, $c=13.273(4)$ Å) containing six units. The asymmetric unit contained three crystallographically independent molecules of **11**. Owing to the physical properties of the crystal, only the iridium and oxygen atoms were refined anisotropically. Figure 2 shows one of the three independent molecules that displays square-planar coordination geometry about the iridium center, thus confirming the bidentate coordination mode of **1a**[14] with a bite angle of 77.3(7)°. The greatest deviation from the plane fitted through the Ir, O, and N atoms and the midpoints of the coordinated C=C double bonds is 0.09 Å for the oxygen atom. The 2,6-dimethylarene is twisted out of the N-Ir-O plane by 91°. The Ir–O bond length (2.102(19) Å) is quite short and comparable to the length of a single Ir–O bond.[9,15,16] The DMA-iridium chelate ring is slightly puckered (a comparison with the DMA-*amine* analogue **19** is presented in Table 1), whereas the C(11) atom is perfectly coplanar with the C(12), C(13), and N atoms, thus precluding any significant charge delocalization from the metal into the π^* orbital of the C=N double bond.

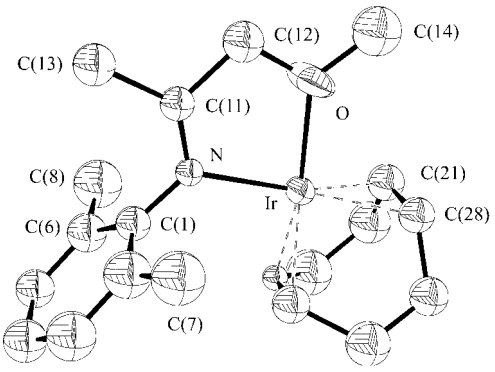

Figure 2. ORTEP view of one of the three independent cationic molecules of **11** (30% thermal ellipsoids). Selected bond lengths [Å] and angles [°]: Ir–O 2.102(19), Ir–N 2.148(16), Ir–C(21) 2.11(3), Ir–C(24) 2.00(2), Ir–C(25) 2.07(3), Ir–C(28) 2.17(2), O–C(12) 1.41(3), C(11)–C(12) 1.55(4), N–C(11) 1.27(3), O-Ir-N 77.3(7), Ir-O-C(12) 119.9(13), Ir-N-C(11) 116.2(16), O-C(12)-C(11) 104(2), N-C(11)-C(12) 123(2).

Table 1. Distances [Å] from the plane defined by O, Ir, and N in complexes **11** and **19**. In the ORTEP plots, the cod ligands and *o*-methyl groups of the aromatic rings are omitted for clarity.

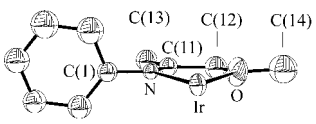

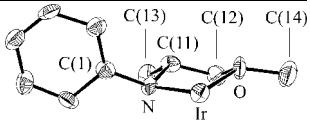

	11	**19**
C(1)	0.008	−0.723
C(11)	−0.108	−0.183
C(12)	−0.147	0.452
C(13)	−0.222	0.374
C(14)	0.092	0.462

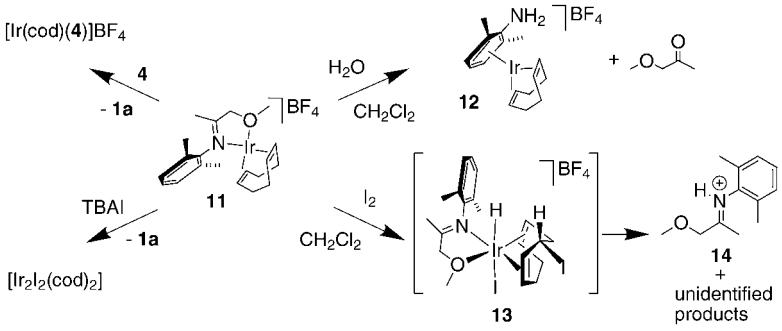

Scheme 3. Reactivity of DMA-imine complex **11**.

An attempt to substitute the cod ligand by treating **11** with a large excess of imine **1a** to form a homoleptic complex under 50 bar hydrogen pressure resulted in the liberation of imine and the precipitation of metallic iridium. To produce an amide that would serve as a model for the postulated intermediate **6** (Scheme 2), **11** was reacted with $Na[HBEt_3]$ ("superhydride") in toluene solution. This resulted in de-coordination of the imine and formation of a mixture of unidentified iridium hydrides. Diphosphine **4** displaced the imine ligand **1a** from complex **11** upon mixing to yield the cationic diphosphine iridium complex $[Ir^I(\mathbf{4})(cod)]BF_4$, which was characterized elsewhere, including an X-ray crystal structure[9] (Scheme 3). Addition of an equimolar amount of TBAI again led to free imine and $[Ir_2I_2(cod)_2]$.[17] Complex **11** reacted with one equivalent of I_2 in CH_2Cl_2 to form quantitatively (NMR spectroscopy) the iminium salt **14**, which was identical to a sample prepared by adding HBF_4 to **1a**,[9] along with other sparingly soluble, unidentified products. We speculate that iminium **14** formed via intermediate **13** in analogy to a published enantioselective C–H activation/iodination of the cod ligand that was achieved by treating $[Ir^I(\mathbf{4})(cod)]BF_4$ with iodine in CH_2Cl_2.[18] In that study we were able to isolate and fully characterize a complex (including an X-ray crystal structure) corresponding to the postulated intermediate **13**, the only difference being the supporting diphosphine ligand **4** instead

of imine **1a**. We propose isomer **13** based on *trans*-influence arguments that justify C–H activation/iodination taking place *trans* to the N donor. Ir^{III} hydrides, such as the postulated intermediate **13**, are acidic and readily deprotonated intramolecularly by imine **1a** to leave a reactive Ir^{I} fragment.[19] Two equivalents of H_2O reacted with **11** over three days in CH_2Cl_2 to afford quantitatively the η^6-dimethylaniline Ir^{I} complex **12** and methoxyacetone. Complex **12** was isolated as a white, air- and water-stable solid and its ^1H NMR spectrum showed the aromatic proton signals of the dimethylaniline ligand shifted to higher fields. Crystals suitable for X-ray crystallography were grown from a CH_2Cl_2/pentane mixture. Figure 3 reveals the η^6 bonding mode of

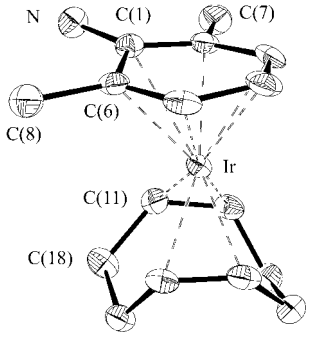

Figure 3. ORTEP view of the cationic part of **12** (BF_4^- omitted, 30% thermal ellipsoids). Selected bond lengths [Å] and angles [°]: Ir–C(1) 2.421(7), Ir–C(2) 2.259(7), Ir–C(3), 2.270(7), Ir–C(4) 2.316(9), Ir–C(5) 2.236(8), Ir–C(6) 2.306(7), N–C(1) 1.363(10), C(1)–C(2) 1.421(10), C(2)–C(3) 1.406(12), C(3)–C(4) 1.416(14), C(4)–C(5) 1.392(14), C(5)–C(6) 1.431(11), N-C(1)-C(2) 119.1(7), N-C(1)-C(6) 121.6(7).

2,6-dimethylaniline and its puckered ring, with C(1) being the atom that deviates most from planarity (0.10 Å). The resulting envelope conformation is characterized by an angle of 15° between the bisecting planes defined by C(1)-C(2)-C(6) and by the best fit through C(2)-C(3)-C(4)-C(5)-C(6). This best plane is 1.79 Å from the iridium center. Two N···F contacts between the N atom and two BF_4^- ions, two sp^3-C···F contacts between C(8) and C(18) and one BF_4^-, an sp^2-C···F contact between C(3) and a fourth BF_4^-, all fall in the range of 3.2–3.4 Å and may indicate weak hydrogen bonding.[20] Crystallographically characterized Ir–η^6-arene complexes are rare[21,22] and the structure of a Rh^{III} η^6-aniline complex has been reported.[23]

Synthesis and reactivity of chiral DMA-amine complexes: Enantiomerically pure (*R*)-**2a** was prepared starting from (*S*)-methyllactate (Scheme 4). Amine **15** was obtained in acceptable yield by analogy to a published procedure.[5] Reduc-

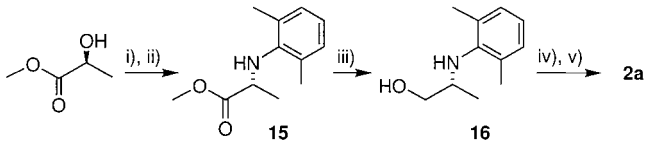

Scheme 4. Synthesis of enantiomerically pure (*R*)-DMA-amine: i) *p*-Nos-Cl, ii) 2,6-dimethylaniline, iii) $LiAlH_4$/THF, iv) KH, 273 K, v) CH_3I/THF.

tion with $LiAlH_4$ in THF gave enantiomerically pure **16** in excellent yield, which was easily methylated[24] to afford (*R*)-**2a** in 75% yield and $\leq$99% *ee*.[25] The specific optical rotation ($[\alpha]_D^{20} = -22.3$, $c = 3.05$ in hexane) is in accordance with the value measured on an optically pure sample that was obtained by a long series of recrystallizations.[26]

Two equivalents of (*R*)-**2a** reacted on a gram-scale with $AgBF_4$ in toluene solution to afford the white microcrystalline silver complex [Eq. (4)] in a high yield in analogy to the synthesis of complex **10** [Eq. (2)].

$$AgBF_4 + 2\,\mathbf{2a} \xrightarrow{\text{toluene}} [Ag(\mathbf{2a})_2]BF_4\ (\mathbf{17}) \qquad (4)$$

(*R*)-**17** showed good solubility in toluene and particularly in CH_2Cl_2 (although with limited stability as in **10**). In the ^1H NMR spectrum, a large downfield shift of the amine proton was observed, resonating at $\delta = 4.82$ ppm (cf. $\delta = 3.4$ ppm in free **2a**), whereas the signals of the methoxy protons of the coordinated amine were shifted upfield. The specific optical rotation is larger and of opposite sign as compared to that of the free amine **2a**: $[\alpha]_D^{20} = +48$ ($c = 0.622$, CH_2Cl_2). Complex **17** cleanly transmetalated with $[Ir_2Cl_2(cod)_2]$ in THF at room temperature to afford a white microcrystalline solid in >80% isolated yield. Surprisingly, this compound displayed no optical activity, and the ^1H NMR spectrum showed an upfield shift of the signals of the aromatic protons of up to 0.8 ppm with respect to that of **2a**. The methoxy protons resonated at higher field ($\delta = 3.34$) relative to those of the DMA-imine complex **11** and approached the value of the free amine **2a** ($\delta = 3.37$ ppm), thus suggesting an uncoordinated methoxy ether function. These observations and the fact that the compound displayed low reactivity pointed to the formation of an 18-valence electron complex with the dimethylaniline ring coordinated in η^6

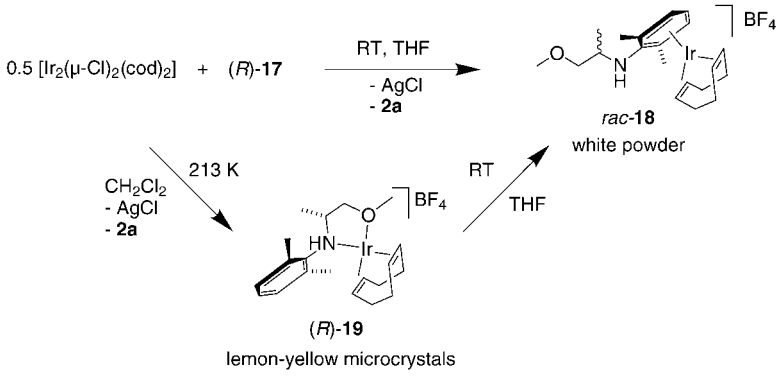

Scheme 5. Syntheses of iridium DMA-amine complexes.

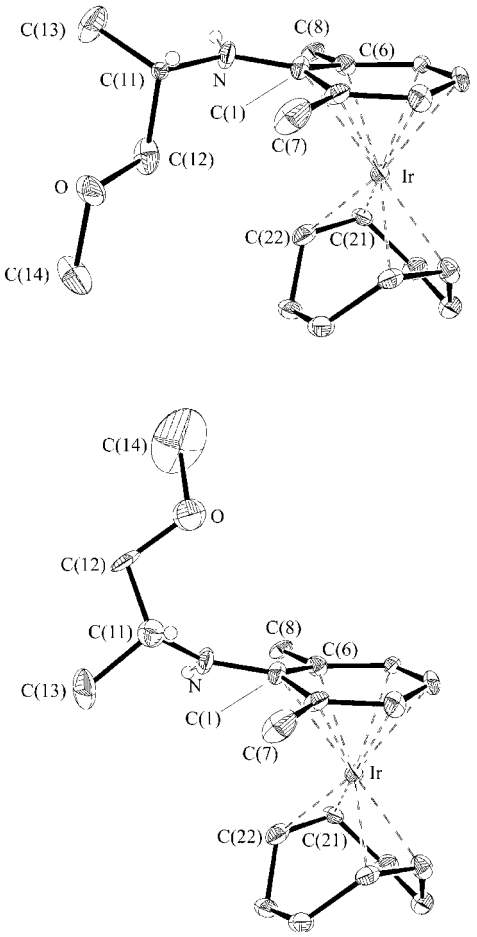

Figure 4. ORTEP view of the two cationic conformers of *rac*-**18** (30% thermal ellipsoids). The H atoms on N and C(11) are in calculated positions and of arbitrary size. Selected bond lengths [Å] and angles [°] (figures in square brackets indicate the corresponding bonding parameters for the disordered sidearm of conformer **B**): Ir–C1 2.448(11), Ir–C(2) 2.314(11), Ir–C(3) 2.217(10), Ir–C(4) 2.289(11), Ir–C(5) 2.270(11), Ir–C(6) 2.250(12), Ir–C(21) 2.134(11), Ir–C(22) 2.136(12), Ir–C(25) 2.134(12), Ir–C(26) 2.156(12), N–C(1) 1.358(13), N–C(11) 1.52(2) [139(3)], C(21)–C(22) 1.44(2), C(25)–C(26) 1.40(2), C(1)–C(2) 1.45(2), C(2)–C(3) 1.41(2), C(3)–C(4) 1.39(2), C(4)–C(5) 1.39(2), C(5)–C(6) 1.430(15), C(1)–C(6) 1.45(2), C(11)–C(12) 1.52(4)[144 (4)], C(11)–C(13) 1.49(4) [158(5)], C(12)–O 1.46(3) [143(4)], O–C(14) 1.45(4) [145(6)], C(1)-N-C(11) 125.6(11) [132.6(14)], N-C(11)-C(13) 110(2) [106(3)], N-C(11)-C(12) 104.5(16) [116(2)], C(12)-C(11)-C(13) 112(3) [110(3)], N-C(1)-C(2) 126.4(10), N-C(1)-C(6) 116.7(10), C(1)-C(2)-C(3) 118.8(10), C(2)-C(3)-C(4) 123.7(10), C(3)-C(4)-C(5) 118.7(9), C(4)-C(5)-C(6) 120.1(10), C(5)-C(6)-C(1) 120.2(9), C(11)-N-C(1)-C(2) −5.6 [38.1].

fashion. This was confirmed by an X-ray crystal structure analysis (Figure 4, vide infra) which allowed us to draw structure *rac*-**18** in Scheme 5. Furthermore, we succeeded in isolating in excellent yield the corresponding κ^2 complex (*R*)-**19** by reacting $[Ir_2Cl_2(cod)_2]$ with **17** in CH_2Cl_2 at 213 K. (*R*)-**19** is a bright yellow solid which maintained optical activity ($[\alpha]_D^{20} = 178$, $c = 0.950$ in CH_2Cl_2). Indeed, the ^1H NMR data pointed towards a bidentate N–O coordination of the amine **2a**: the amine proton resonated at $\delta = 5.61$ ppm, downfield by 2.2 ppm with respect to that of free **2a**. Similarly, the methoxy protons resonated at lower field than in **2a**, and the aromatic protons resonated in the normal range. Finally, an X-ray diffraction study confirmed the proposed

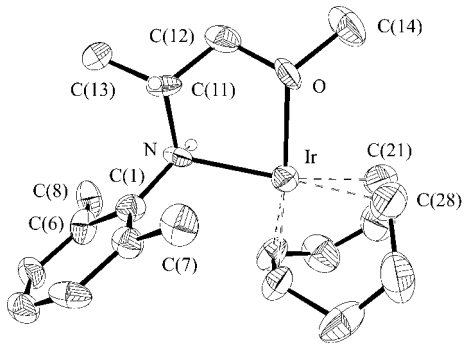

Figure 5. ORTEP view of the cation of (*R*)-**19** (30% thermal ellipsoids). The H atoms on N and C(11) are in calculated positions. Selected bond lengths [Å] and angles [°]: Ir–O 2.116(10), Ir–N 2.135(11), Ir–C(21) 2.10(2), Ir–C(22) 2.08(2), Ir–C(25) 2.06(2), Ir–C(26) 2.084(14), O–C(12) 1.44(2), O–C(14) 1.44(2), N–C(1) 1.40(2), N–C(11) 1.51(2), C(11)–C(12) 1.47(2), C(11)–C(13) 1.53(2), C(21)–C(22) 1.41(3), C(25)–C(26) 1.37(3), O-Ir-N 79.6(4), O-Ir-C(21) 97.6(6), O-Ir-C(22) 95.4(7), O-Ir-C(25) 161.8(6), O-Ir-C(26) 158.5(7), N-Ir-C(21) 156.4(6), N-Ir-C(22) 163.5(7), N-Ir-C(25) 97.4(6), N-Ir-C(26) 93.1(5), Ir-N-C(11) 109.3(8), Ir-N-C(1) 119.0(8), Ir-O-C(12) 111.5(8), Ir-O-C(14) 125.0(10), N-C(11)-C(12) 110.8(13), N-C(11)-C(13) 110.6(12), Ir-N-C(1)-C(2) 59.1, C(11)-N-C(1)-C(2) −72.1.

bonding mode (Figure 5). Reactivity studies showed κ^2-bound **2a** to be very labile and (*R*)-**19** was soluble and moderately stable only in CH_2Cl_2. Complex *rac*-**18** was independently synthesized in good yield by refluxing a THF solution of (*R*)-**19** (Scheme 5). The kinetics of this reaction are discussed below. Addition of chiral diphosphine **4** to CD_2Cl_2 solutions of **18** and **19** displaced amine **2a** over a period of two days and upon mixing, respectively, to form complex $[Ir^I(\mathbf{4})(cod)]BF_4$. DMA-imine **1a** did not displace amine **2a** in complex **18**, whereas the reaction with **19** quantitatively produced DMA-imine complex **11** and free DMA-amine during the time of mixing. The kinetics of this amine/imine exchange are presented below and served as a model reaction for the final step in the proposed catalytic cycle depicted in Scheme 2 (vide supra).

Crystals of *rac*-**18** were grown from a saturated THF solution. Its X-ray structure confirmed the total racemization of the coordinated DMA-amine (Figure 4). Complex *rac*-**18** crystallizes in the space group $P\bar{1}$ with one molecule in the asymmetric unit. The side arm is statistically disordered over two positions with 50% occupancy and with opposite stereochemistries at C(11). The bond lengths along the side chains should be interpreted with caution in view of their disorderly behavior. The atoms C(11A) and C(11B) were refined with isotropic thermal parameters. Figure 4 shows the two enantiomers **A** and **B** with a selection of bond parameters. Molecule **A** displays a somewhat puckered η^6-coordinated arene moiety and, attached to it, the aliphatic chain oriented towards the cod–Ir–arene core. As expected, there are no intramolecular or intermolecular interactions between the free amine and ether functions with the iridium center. The conformation of the η^6-coordinated arene is best described as an envelope defined by the C(1)-C(2)-C(6) plane and the best plane through C(2)-C(3)-C(4)-C(5)-C(6). The interplanar angle is 14°. The iridium atom is 1.778 Å

from the above-defined best plane. The C1–N vector (1.358 Å) is 0.04 Å shorter than in **19** and lies within the C(1)-C(2)-C(6) plane. The C(1)-N-C(11) bond angle (126°) is almost 12° larger than in $\widehat{NO}$-coordinated DMA-amine. Furthermore, the C(11)–N bond is approximately coplanar with the arene, as indicated by the C(11)-N-C(1)-C(2) torsion angle of −5.6°. This same torsion angle is much larger (−72.1°) when the DMA-amine is $\widehat{NO}$ bound to iridium (**19**). Thus, it appears that a third large substituent on the N atom (be it the iridium fragment in **19** or the chloroacetyl unit in Metolachlor[5]) causes the out-of-plane tilting of the arene ring.

Compound **19** crystallized from a CH_2Cl_2/Et_2O mixture. Figure 5 reveals the square-planar coordination environment in complex (*R*)-**19** and provides a selection of bond parameters. The DMA-amine bite angle of 79.6(4)° is slightly larger than the corresponding angle in the imine complex **11**. The largest deviation from the best plane defined by the Ir, O, and N atoms and by the midpoints of the coordinated olefins is −0.08 Å for the center of the C(21)=C(22) bond and is comparable to that found in the imine adduct **11**. The Ir–O bond length is fairly short (2.116(10) Å) and the Ir–N bond length of 2.135(11) Å lies in the expected range when compared to the few examples of structurally characterized Ir^I amine complexes.[27–29] No significant difference in the *trans* influences of the O and N atoms on the coordinated olefins is observed. The five-membered ring formed by Ir, N, C(11), C(12), and O adopts a half-chair conformation. Naturally, the DMA-amine ligand is more puckered than the DMA-imine ligand, and a comparison with **11** is presented in Table 1.

Kinetics of the DMA-amine/DMA-imine exchange on iridium: The ligand-exchange reaction of Equation (5) was monitored by means of the stopped-flow technique. Note that Equation (5) models the upper part of the cycle in Scheme 2 and relates intermediates **7** and **5**.

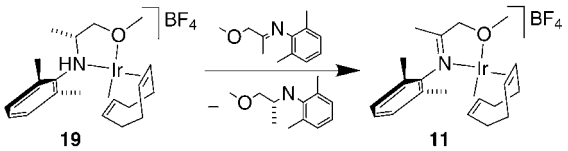

(5)

First, the optical spectra of **1a**, **11**, and **19** in CH_2Cl_2 were recorded to find the optimum wavelength for the stopped-flow experiments (Figure 6). At $\lambda = 360$ nm and 424 nm, the difference in absorbance without interference from **1a** was largest, but measurements at 424 nm offered the additional advantage of a slightly superior instrument performance (lower noise level). The amine complex (initial concentration of 3.59×10^{-4} M throughout) was allowed to react at 298 K with 10-, 20-, 40-, and 80-fold excesses of imine to warrant pseudo-first-order conditions for the initial reaction step for easier interpretation. The temperature dependence of the reaction rate was investigated between 276 K and 308 K with an 80-fold excess of imine.

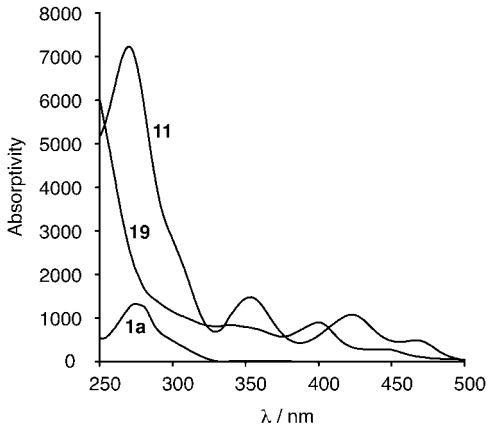

Figure 6. UV/Vis spectra of **1a**, **11**, and **19** in CH_2Cl_2.

The traces obtained at 298 K at variable imine excesses show that the reaction occurs in at least two significant steps. If there were only one rate-determining step, neat exponential curves would be expected at such large imine excesses. The change in the shape of the trace with increasing imine excess suggests the existence of additional slow steps (Figure 7). Two steps are well-separated, even at the lowest

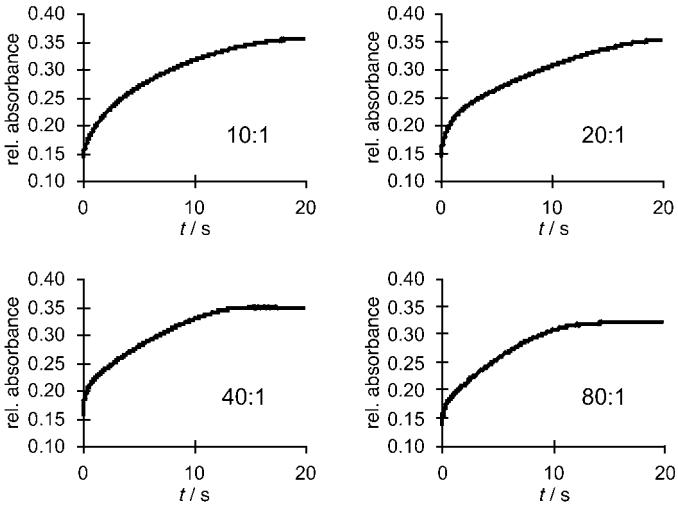

Figure 7. Traces of the reaction of **19** with varying excesses of **1a** recorded at $\lambda = 424$ nm.

imine excess, and the rate of the first step is obviously concentration-dependent, since the rise of the curve becomes steeper with a larger imine excess. It follows that this first step is bimolecular and, therefore, most likely represents the addition of an imine molecule to the amine complex **19**. The second step cannot be assigned unambiguously with a simple two-step model. If the second step were independent of the imine concentration, the second phase of the traces would be equal in all cases. If it were dependent on the imine concentration, the total reaction time would shorten with increasing imine concentration although the shapes of the traces would remain geometrically similar. This is almost the case for ratios of **1a**:**19** of 20:1, 40:1, and 80:1, but not

exactly. The final absorbance would also remain constant for a given concentration of complex **19** because this would limit the amount of product. The observed diminished final absorbance suggests the formation of additional species at large imine excesses. The traces were first coarsely analyzed with the assumption of a two-step forward reaction (described by k_1 and k_2) using Monte Carlo and Newton–Gauss algorithms to fit the integrated differential equations. A more detailed analysis was then carried out by numerical integration of more complex kinetic models in the form of coupled differential equations. The best approximation to the set of traces was found with a final equilibrium in which the product complex **11** acquires an additional imine molecule in a two-step process (characterized by k_3/k_{-3} and k_4/k_{-4}, Scheme 6). The diminished absorbance at the end of the traces is mainly caused by k_4/k_{-4}. The traces were simulated with the known extinction coefficients from the spectra in Figure 6. If more than two forward steps are allowed in the model, the rate of the second step is found to be independent of the initial imine concentration, and most probably represents the elimination of the amine. The standard deviation (2σ) of the second rate constant becomes smaller if it is assumed that the first step is reversible (introducing k_{-1}). This is reasonable for an addition reaction to a square-planar complex. The values found for the bimolecular imine addition and the amine elimination rate constants are $(2.6\pm 0.3)\times 10^2\,\text{M}^{-1}\,\text{s}^{-1}$ and $(4.3\pm 0.6)\times 10^{-2}\,\text{s}^{-1}$, respectively. Given the method of approximation and the uncertainties about the properties of the minor products, these values are reliable within their decades. The equilibrium constant of the imine addition is estimated to be $1.5\times 10^4\,\text{M}^{-1}$. The precise rate constants of the forward and backward reactions of this equilibrium cannot be determined because the equilibrium settles faster than the preceding reaction proceeds.

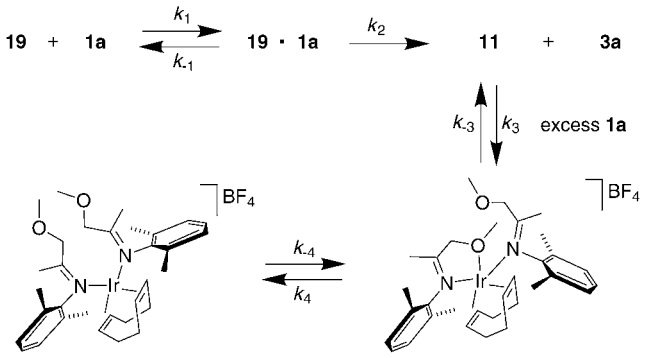

Scheme 6. Kinetic model used to determine k_1 and k_2.

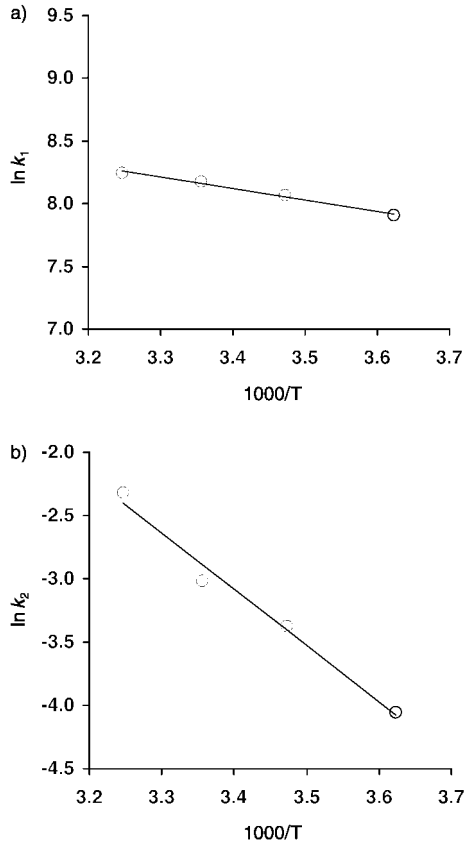

Figure 8. Arrhenius plots of the first (a) and second step (b) of the reaction of **19** with **1a**.

The activation energies for the first two distinct reaction steps were determined by varying the temperature from 276 K to 308 K (Figure 8). Step 1 requires a low activation energy of $7.5\pm 0.6\,\text{kJ mol}^{-1}$, as expected for an addition reaction to a free coordination site. Step 2 has a considerably higher activation energy of $37\pm 3\,\text{kJ mol}^{-1}$, which points to an intramolecular rearrangement. The frequency factors obtained from a narrow temperature range must be interpreted with caution, although some qualitative information may be deduced in the case of large differences. Frequency factors of $7.2\times 10^4\,\text{s}^{-1}$ and $1.7\times 10^5\,\text{s}^{-1}$ were estimated for the first and second steps, respectively, and are of comparable magnitude. The difference in the relative velocities of the two steps (addition and elimination) is thus mainly determined by the respective activation energies.

Racemization via C–H activation: Dissolution of (*R*)-**19** in THF led to the clean formation of *rac*-**18** over two days at room temperature (Scheme 5), while solutions of (*R*)-**19** in CH_2Cl_2 were stable. The disappearance of (*R*)-**19** and the appearance of *rac*-**18** went hand-in-hand with a diminishing optical activity of the THF solution. This decay was monitored by optical rotation spectrometry and NMR spectroscopy.

Figure 9 shows the evolution of the $[\alpha]_D$ of a THF solution of (*R*)-**19** over 700 minutes. A good fit was obtained with the reaction sequence shown in Scheme 7. The first step is probably pseudofirst order, namely, $k_1' = k_1[\text{THF}]$ with $k_1' = 9.0\times 10^{-4}\,\text{s}^{-1}$, whereas the second step is first order with $k_2 = 2.89\times 10^{-5}\,\text{s}^{-1}$. From the data at hand, we found the intermediate to be optically active with an $[\alpha]_D = 163\pm 9$. No hydride signals were detected in the NMR spectra during the reaction. We postulate an intermediate such as **20** (Scheme 7), in which the ether function of the amine is displaced by an incoming THF molecule. This should render the βH atom on the stereogenic carbon atom more accessible to the iridium center. Thus, the racemization of amine

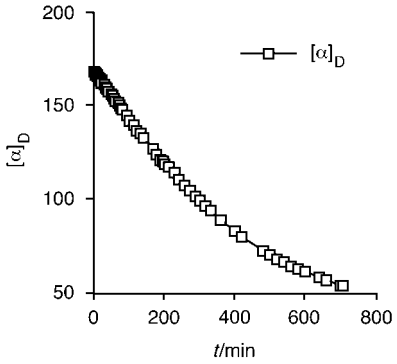

Figure 9. $[\alpha]_D$ as a function of time. Measured 5 min after dissolving (*R*)-**19** in THF at 298 K.

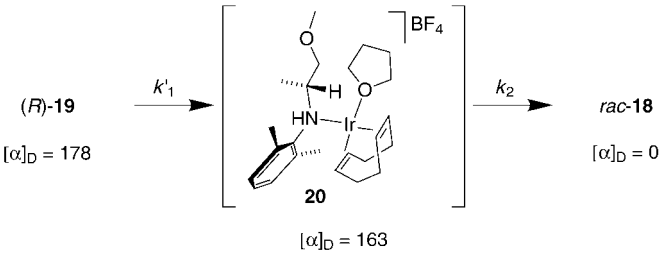

Scheme 7. Proposed intermediate DMA-amine complex prior to C–H activation.

2a probably occurs by reversible sp^3 C–H activation (βH elimination to afford an intermediate iminium species **14**, followed by re-insertion into the Ir–H bond). It should be noted that C–H activation by oxidative addition is usually accomplished by electron-rich late transition metal centers bearing electron-donating ligands, such as phosphines or cyclopentadienyl anions. The coordinated amine function of **2a** augments the electron density on the Ir^I center and thus seems to render C–H bond activation feasible. Pre-coordination of an amine function to an Ir^I species triggering C–H[30] and N–H[31] activation is documented, and the activation of a C–H bond α to a amine function by a Ir^I(cod) fragment has been demonstrated by deuterium labeling experiments.[29] This racemization reaction may explain why the stereoselectivity of the hydrogenation of **1b** is limited to $\approx$80%, and it points to a potential mechanism of catalyst deactivation. In fact, *rac*-**18** turned out to be a very stable and inert 18 valence electron complex. The elucidation of the precise mechanism needs further studies.

To summarize, we succeeded in synthesizing and characterizing imine and optically pure amine complexes of Ir^I that are relevant to the Syngenta MEA-imine hydrogenation process. We showed that the DMA-imine and DMA-amine molecules (as very close models to MEA-imine and MEA-amine) indeed exhibited all coordination modes conceivable based on their structure (Figure 1). Bidentate $\widehat{NO}$ coordination to iridium was demonstrated for the DMA-imine (complex **11**) and the DMA-amine molecule (complex **19**). In both complexes, switching of the coordination mode from κ^2-$\widehat{NO}$ to η^6-arene were observed upon hydrolysis of **11** and racemization of **19** leading to **12** and **18**, respectively. An important part of the hydrogenation cycle (i.e. product–substrate exchange) was modeled, and the kinetic data suggest that imine **1a** displaces amine **2a** from complex **19** by an associative mechanism. The substrate molecule (imine **1a**) is indeed the much better ligand for Ir^I than the product molecule (amine **2a**). In fact, the industrial solvent-free MEA-imine hydrogenation proceeds rapidly and to completion, despite the very large MEA-amine concentration toward the end of the reaction.[32] Indirect evidence for sp^3-C–H activation was found in two cases: In the I_2 oxidation of complex **11**, leading to one equivalent of iminium salt **14** (via the proposed C–H activated intermediate **13**), and in the racemization of (*R*)-**19**, leading to *rac*-**18** (via β-C–H activation of the amine by the Ir^I(cod) fragment). The latter transformation of κ^2-coordinated amine (*R*)-**2a** into racemic, η^6-coordinated *rac*-**2a** bears some relevance to the industrial process. It demonstrates that an iridium catalyst is, in principle, capable of lowering the optical purity of the product amine by sp^3-C–H bond activation,[33] and it shows a possible catalyst deactivation pathway by η^6 coordination of substrate or product molecules that irreversibly block coordination sites on the iridium catalyst. Hydrolysis of the iridium-coordinated imine substrate molecule to afford an η^6-bonded dialkylaniline iridium complex, as observed in the formation of complex **12**, is a slow reaction and unlikely to occur during the fast imine hydrogenation reaction. In both cases, the Ir^I(cod) fragment showed a strong tendency to coordinate the aniline fragment in an η^6 fashion.

Experimental Section

$[Ir_2Cl_2(cod)_2]$,[34] **1a**, and **10**[9] were synthesized according to published procedures. All reactions were carried out under anaerobic and anhydrous conditions and reactions involving Ag salts were carried out in the dark. Elemental analyses were performed at the Mikroelementaranalytisches Laboratorium, ETH Zürich. Optical rotation spectra were recorded on a Perkin-Elmer 341 polarimeter, and optical spectra were recorded on a Uvikon 820 spectrophotometer. The stopped-flow experiments were performed on a Applied Photophysics SX17MV instrument under anaerobic conditions. The thermostat fluid was continuously purged with nitrogen (99.999%), and the rear side of the array of drive syringe pistons was covered with a nitrogen-purged cap. The reactant solutions (**19** and **1a** in CH_2Cl_2) were supplied from tonometer reservoirs (Schlenk tube-like vessels) which were filled in a glove box. The concentration of **19** was 3.5×10^{-4} M throughout, and that of **1a** was 3.5×10^{-3} M, 7×10^{-3} M, 1.4×10^{-2} M, and 2.8×10^{-2} M. In the temperature-dependence experiments, the concentration of **1a** was 2.8×10^{-2} M throughout. Recording of valid traces was started after the stopped-flow circuit had been flushed with reactants until the trace shape became stable. The traces were analyzed with the built-in fit capabilities of the Applied Photophysics control software and subsequently with the program proFit (Quantum Soft, Zürich, Switzerland). The more complex analyses were carried out by numerical integration in a Microsoft Excel spreadsheet. Integration was effected by a VBA macro which uses a 4th order Runge–Kutta algorithm. The fit to the experimental data was calculated with the built-in Solver macro in the tangent mode.

[Ir(cod)(κ^2-1a)]BF_4 (11): THF (250 mL) was added to $[Ir_2Cl_2(cod)_2]$ (1.007 g, 1.499 mmol) and $[Ag(\mathbf{1a})_2]BF_4$ (**10**, 1.730 g, 2.997 mmol). The resulting green-yellow mixture was stirred for 1 h and then evaporated to dryness. The residue was extracted with CH_2Cl_2 (4×20 mL). The volatiles were evaporated, and the residue was washed in Et_2O (3×80 mL) and dried in vacuo to afford a greenish-yellow powder. Yield: 1.680 g (97%); ^{1}H NMR (250.13 MHz, CD_2Cl_2): δ = 1.43 (br, 2H), 1.70 (br, 2H), 1.90 (s,

3H), 2.20 (br, 4H), 2.22 (s, 6H), 2.80 (br, 2H), 3.95 (s, 3H), 4.34 (br, 2H), 5.39 (s, 2H), 7.13–7.18 ppm (m, 3H); elemental analysis calcd (%) for $C_{20}H_{29}NBOF_4Ir$: C 41.53, H 5.05, N 2.42; found: C 41.47, H 5.23, N 2.36.

Methyl-(2*S*)-*O*-(*p*-nitrobenzenesulfonyl)lactate: A stirred solution of (*S*)-methyllactate (113.4 g, 1.089 mol) and *p*-nitrobenzenesulfonyl chloride (100.0 g) in ethyl acetate (0.50 L) was treated with NEt_3 (69 mL). The temperature was kept below 300 K. The resulting white slurry was stirred overnight and then heated to 333 K for 1 h. After filtration, the organic phase was washed with HCl (2 M), H_2O, NaOH (2 M), and brine. The organic phase was dried over Na_2SO_4, and the volatiles were evaporated. The residue was dissolved in CH_3OH (80 mL), and the solution was cooled to afford an off-white crystalline solid that was collected by filtration and dried in vacuo (63.6 g, 20%).

(*R*)-*N*-(1′-Methyl-2′-methylcarboxyethyl)-2,6-dimethylaniline (15): To a stirred yellow solution of 2,6-dimethylaniline (111 mL, 0.900 mmol) in chlorobenzene (400 mL) was added dropwise a solution of methyl-(2*S*)-*O*-(*p*-nitrobenzenesulfonyl)lactate (160 g, 0.552 mol) in chlorobenzene (160 mL) at reflux temperature. The mixture was refluxed for a further 4 h to afford a red solution. After filtration of the solution and evaporation of the volatiles, the oily residue was washed with HCl (1 M) and extracted with Et_2O. Drying over Na_2SO_4 and distillation afforded a yellow oil. Yield: 48.7 g (45%); $[\alpha]_D^{20} = 37.8$ ($c = 1.25$, CH_3OH).

(*R*)-*N*-(1′-Methyl-2′-hydroxyethyl)-2,6-dimethylaniline (16): To a pale yellow solution of (*R*)-*N*-(1′-methyl-2′-methylcarboxyethyl)-2,6-dimethylaniline (**15**, 4.45 g, 21.4 mmol)in THF (100 mL) was added a ≈1 M solution of $LiAlH_4$ (21.5 mL, 21.5 mmol) in THF dropwise over 15 min by a syringe. The solution was stirred for 6 h, and it changed color from dark yellow to pale yellow. The mixture was quenched by adding i) H_2O (0.8 mL), ii) aq. NaOH (0.8 mL, 15%), iii) H_2O (1.6 mL), and iv) ≈1 g of Na_2SO_4 to the vigorously stirred solution. The salts were filtered off and washed with Et_2O. The volatiles of the combined organics were removed in vacuo. The resulting oil was redissolved in CH_2Cl_2 and washed with H_2O (2×50 mL). The organic phase was dried with Na_2SO_4 and then distilled (2×10^{-2} mbar, $T_{vap} \approx 359$ K) to afford a pale yellow, highly viscous oil. Yield: 3.29 g (86%); $[\alpha]_D^{20} = +7.24$ ($c = 1.974$, CH_3OH); ^1H NMR (250.13 MHz, $CDCl_3$): $\delta = 1.07$ (d, 6.3 Hz, 3H), 2.30 (s, 6H), 2.49 (br, 1H), 2.94 (br, 1H), 3.35–3.55 (m, 2H), 3.65–3.75 (m, 1H), 6.80–6.85 (m, 1H), 7.00–7.05 ppm (m, 2H); elemental analysis calcd (%) for $C_{11}H_{17}NO$: C 73.7, H 9.56, N 7.81; found: C 73.6, H 9.51, N 7.87.

(*R*)-*N*-(1′-methyl-2′-methoxyethyl)-2,6-dimethylaniline ((*R*)-2a): A solution of (*R*)-*N*-(1′-methyl-2′-hydroxyethyl)-2,6-dimethylaniline (**16**, 1.983 g, 11.06 mmol) in THF (35 mL) was added dropwise over 10 min to a stirred suspension of KH (0.475 g, 11.8 mmol) in THF (15 mL). H_2 evolution was observed. The mixture was stirred overnight at room temperature to afford a turbid yellow solution. A solution of CH_3I in THF (20 mL) was added dropwise over 80 min under vigorous stirring. Large amounts of a white precipitate formed. The mixture was concentrated to 30 mL, and brine (100 mL) was added. Extraction of this mixture with Et_2O and distillation (10^{-2} mbar, $T_{vap} \approx 318$ K) yielded a yellowish viscous oil. Yield: 1.58 g (75%); $[\alpha]_D^{20} = -22.3$, $[\alpha]_{365}^{20} = -129$ ($c = 3.05$, hexane); ^1H NMR (250.13 MHz, $CDCl_3$): $\delta = 1.19$ (d, $J = 6.4$ Hz, 3H), 2.28 (s, 6H), 3.30–3.45 (m, 4H), 3.37 (s, 3H), 6.75–6.85 (m, 1H), 6.95–7.00 ppm (m, 2H); elemental analysis calcd (%) for $C_{12}H_{18}NO$: C 74.96, H 9.44, N 7.28; found: C 74.9, H 9.80, N 7.15.

$[Ag((R)\text{-}2a)_2]BF_4 \cdot {}^1/_8 C_7H_8$ (17): (*R*)-*N*-(1′-Methyl-2′-methoxyethyl)-2,6-dimethylaniline [(*R*)-**2a**, 2.060 g, 10.66 mmol] was added dropwise to a pinkish solution of $AgBF_4$ (1.002 g, 5.147 mmol) in toluene (40 mL). The mixture was stirred for 1 h at room temperature, and then the volatiles were evaporated. The residue was washed with pentane (3×20 mL) and dried in vacuo to afford a white microcrystalline powder. Yield: 2.79 g (91%); ^1H NMR (CD_2Cl_2, 250.13 MHz): $\delta = 0.93$ (d, 6H, $J = 6.1$ Hz), 2.34 (br s, 12H), 2.66 (s, 6H), 3.27–3.50 (m, 6H), 4.82 (br d, 2H), 6.95–7.08 ppm (m, 6H). The NMR spectrum indicated $^1/_8$ equivalents of toluene. $[\alpha]_D^{20} = +48$ ($c = 0.622$, CH_2Cl_2); elemental analysis calcd (%) for $C_{24}H_{38}AgBF_4N_2O_2 \cdot {}^1/_8 C_7H_8$: C 50.40, H 6.63, N 4.73; found: C 50.71, H 6.57, N 4.85.

$[Ir(cod)(\eta^6\text{-}rac\text{-}2a)]BF_4$ (18):

Method A: THF (12 mL) was added to $[Ir_2Cl_2(cod)_2]$ (182.2 mg, 0.271 mmol) and $[Ag((R)\text{-}2a)_2]BF_4 \cdot {}^1/_8 C_7H_8$ (**17**, 321.4 mg, 0.542 mmol) with a syringe. The resulting mixture was stirred at room temperature for 130 h, and the volatiles were removed with a vacuum pump to afford an olive green solid that was extracted with CH_2Cl_2 (3×3 mL). The solution was evaporated to yield a red oily solid that was recrystallized from THF (4 mL) and Et_2O (12 mL) to afford a white microcrystalline solid. Yield: 255 mg (81%). Crystals suitable for an X-ray analysis were obtained by dissolving 95 mg of the product in THF (1.2 mL) at 333 K and then leaving the solution at room temperature for two days. $[\alpha]_D^{20} = 0$ ($c = 0.546$, CH_2Cl_2); elemental analysis calcd (%) for $C_{20}H_{31}NBOF_4Ir$: C 41.38, H 5.38, N 2.41; found: C 41.20, H 5.26, N 2.34.

Method B: A THF solution (5 mL) of $[Ir(cod)((R)\text{-}2a)]BF_4$ ((*R*)-**19**, 99 mg) was refluxed for 20 h, and the mixture was then concentrated to about 1 mL. Addition of Et_2O (7 mL) precipitated an off-white solid. The supernatant solution was filtered off and the solid dried in vacuo. Yield: 82 mg (83%); ^1H NMR (250.13 MHz, CD_2Cl_2): $\delta = 1.32$ (d, 3H, $^3J = 6.6$ Hz), 2.00–2.30 (m, 8H), 2.13 (s, 3H), 2.17 (s, 3H), 3.35 (s, 3H), 3.44 (m, 2H), 3.95–4.10 (m, 5H), 4.38 (br d, 1H, $J = 9.9$ Hz), 6.15–6.19 (m, 2H), 6.36 ppm (m, 1H); elemental analysis calcd (%) for $C_{20}H_{31}NBOF_4Ir$: C 41.38, H 5.38, N 2.41; found: C 41.13, H 5.41, N 2.47.

$[Ir(cod)(\kappa^2\text{-}(R)\text{-}2a)]BF_4$ ((*R*)-19): A colorless solution of $[Ag((R)\text{-}2a)_2]BF_4 \cdot {}^1/_8 C_7H_8$ (**17**, 628.7 mg, 1.061 mmol) in CH_2Cl_2 (20 mL) was added dropwise to an orange solution of $[Ir_2Cl_2(cod)_2]$ (356.2 mg, 0.5300 mmol) in CH_2Cl_2 (20 mL) at 213 K over 20 min. The resulting lemon-yellow mixture was slowly allowed to reach 273 K over 2.5 h. The mixture was then evaporated to afford a yellow solid that was extracted with CH_2Cl_2 (3×30 mL). Concentration to ≈5 mL and addition of Et_2O (10 mL) caused the precipitation of lemon-yellow microcrystals. Yield: 565 mg (92%); ^1H NMR (250.13 MHz, CD_2Cl_2): $\delta = 1.02$ (br, 1H), 1.11 (d, 3H, $^3J(H,H) = 6.5$ Hz), 1.18 (br, 1H), 1.63 (br, 1H), 1.84 (br, 2H), 2.1–2.6 (br, 4H), 2.43 (s, 3H), 3.09 (s, 3H), 3.45–3.65 (m, 2H), 3.81 (s, 3H), 3.84 (dd, 1H, $^3J = 4.9$ Hz), 4.43 (dd, 1H, $J_{vic} = 11.6$ Hz, $^3J = 9.9$ Hz), 5.61 (br d, 1H, $^3J = 10.7$ Hz), 7.05–7.09 (m, 2H), 7.14–7.19 ppm (m, 1H); $[\alpha]_D^{20} = +178$ ($c = 0.950$, CH_2Cl_2); elemental analysis calcd (%) for $C_{20}H_{31}BF_4IrNO$: C 41.38, H 5.38, N 2.41; found: C 41.44, H 5.52, N 2.40. Crystals suitable for an X-ray analysis were grown by careful layering of a solution of the compound (108 mg) in CH_2Cl_2 (1 mL) with Et_2O (5 mL).

CCDC-223547, CCDC-134959, CCDC-134962, and CCDC-134960 contain the supplementary crystallographic data for compounds **11**, **12**, **18**, and **19**, respectively. These data can be obtained free of charge via www.ccdc.cam.ac.uk/conts/retrieving.html (or from the Cambridge Crystallographic Data Centre, 12 Union Road, Cambridge CB2 1EZ, UK; fax: (+44) 1223-336033; or deposit@ccdc.cam.uk).

Acknowledgement

We thank Dr. Volker Gramlich (ETH) for solving the crystal structure of compound **11**. R.D. thanks Novartis AG (Switzerland) and FONACIT (Venezuela) for financial support.

[1] C. Vogel, R. Aebi, **1972** DP 2328340 to Ciba-Geigy AG.
[2] H.-U. Blaser, F. Spindler, *Chimia* **1997**, *51*, 297.
[3] H.-U. Blaser, H.-P. Buser, K. Coers, R. Hanreich, H.-P. Jalett, E. Jelsch, B. Pugin, H.-D. Schneider, F. Spindler, A. Wegmann, *Chimia* **1999**, *53*, 275.
[4] H.-U. Blaser, *Adv. Synth. Catal.* **2002**, *344*, 17.
[5] H. Moser, G. Rhys, *Z. Naturforsch. B* **1982**, *37*, 451.
[6] Y. Ng Cheong Chan, J. A. Osborn, *J. Am. Chem. Soc.* **1990**, *112*, 9400.
[7] F. Spindler, B. Pugin, H.-U. Blaser, *Angew. Chem.* **1990**, *102*, 561; *Angew. Chem. Int. Ed. Eng.* **1990**, *29*, 558.
[8] D. Xiao, X. Zhang, *Angew. Chem.* **2001**, *113*, 3533; *Angew. Chem. Int. Ed.* **2001**, *40*, 3425.
[9] R. Dorta, D. Broggini, R. Stoop, H. Rüegger, F. Spindler, A. Togni, *Chem. Eur. J.* **2004**, *10*, 267.
[10] G. Fink, R. Mühlhaupt, H. H. Brintzinger, *Ziegler Catalysts*, Springer, Berlin Heidelberg **1995**.

[11] R. Noyori, T. Ohkuma, *Angew. Chem.* **2001**, *113*, 40; *Angew. Chem. Int. Ed.* **2001**, *40*, 40.
[12] D. M. Fryzuk, W. E. Piers, *Organometallics* **1990**, *9*, 986.
[13] F. Spindler (Solvias AG), personal communication.
[14] A. G. Becalski, W. R. Cullen, M. D. Fryzuk, B. R. James, G.-J. Kang, S. J. Rettig, *Inorg. Chem.* **1991**, *30*, 5002.
[15] C. A. Miller, T. S. Janik, C. H. Lake, L. M. Toomey, M. R. Churchill, J. D. Atwood, *Organometallics* **1994**, *13*, 5080.
[16] M. A. Esteruelas, A. M. López, L. A. Oro, A. Péres, M. Schulz, H. Werner, *Organometallics* **1993**, *12*, 1823.
[17] S. M. Socol, C. Yang, D. W. Meek, R. Glaser, *Can. J. Chem.* **1992**, *70*, 2424.
[18] R. Dorta, A. Togni, *Organometallics* **1998**, *17*, 5441.
[19] In the presence of diphosphine ligand **4**, the deprotonated Ir^{I} complex underwent an S_{Ni}-type reaction to form the allyl complex $[IrI(\mathbf{4})(\eta^3,\eta^2\text{-}C_8H_{11})]BF_4$ (see ref. [18]). In the present case, the resulting iridium fragment is poorly supported and thus may form sparingly soluble precipitates.
[20] G. A. Jeffrey, *An Introduction to Hydrogen Bonding*, Oxford University Press, Oxford, New York **1997**.
[21] R. Usón, L. A. Oro, D. Carmona, M. A. Esteruelas, C. Foces-Foces, F. H. Cano, S. Garcia-Blanco, *J. Organomet. Chem.* **1983**, *254*, 249.
[22] J. W. Steed, R. K. Juneja, R. S. Burkhalter, J. L. Atwood, *J. Chem. Soc. Chem. Commun.* **1994**, 2205.
[23] S. Ogo, H. Chen, M. M. Olmstead, R. H. Fish, *Organometallics* **1996**, *15*, 2009.
[24] A. I. Meyers, G. S. Poindexter, Z. Birch, *J. Org. Chem.* **1987**, *52*, 892.
[25] Determined by chiral HPLC using Daicel's Chiracel ODH column and eluting with 2-propanol (0.35%) in hexane; 1.0 mL min^{-1}; T = 298 K; R_f = 7.1 min for (*R*)-**2a**; R_f = 8.2 min for (*S*)-**2a**.
[26] K. Bernauer (University of Neuchâtel, Switzerland), personal communication.
[27] D. M. Roundhill, R. A. Bechtold, S. G. N. Roundhill, *Inorg. Chem.* **1980**, *19*, 284.
[28] C. Bianchini, E. Farnetti, M. Graziani, G. Nardin, A. Vacca, F. Zanobini, *J. Am. Chem. Soc.* **1990**, *112*, 9190.
[29] A. A. H. Van der Zeijden, G. van Koten, R. Luijk, R. A. Nordemann, A. L. Spek, *Organometallics* **1988**, *7*, 1549.
[30] R. Dorta, A. Togni, *Organometallics* **1998**, *17*, 3423.
[31] A. L. Casalnuovo, J. C. Calabrese, D. Milstein, *Inorg. Chem.* **1987**, *26*, 971.
[32] The coordination behavior of the substrate and product molecules may be assumed to be similar in the Ir^{I}(cod) fragment and in the actual catalyst system (based on the Ir^{III}(xyliphos) fragment, see ref. [9]).
[33] A comprehensive ligand screening revealed that it is difficult to reach 90% *ee*. F. Spindler (Solvias AG), personal communication.
[34] R. H. Crabtree, Q. J. M. , H. Felkin, T. Fillebeen-Kahn, *Synth. React. Inorg. Met.-Org. Chem.* **1982**, *12*, 407.

Received: December 10, 2003
Revised: April 14, 2004
Published online: August 2, 2004

